Self-Assembled Gold Nanoparticle/Alkanedithiol Films: Preparation, Electron Microscopy, XPS-Analysis, Charge Transport, and Vapor-Sensing Properties†

Yvonne Joseph,§ Isabelle Besnard,§ Miriam Rosenberger,§ Berit Guse,§ Heinz-Georg Nothofer,§ Jurina M. Wessels,§ Ute Wild,‡ Axel Knop-Gericke,‡ Dangsheng Su,‡ Robert Schlögl,‡ Akio Yasuda,§ and Tobias Vossmeyer*,§

Materials Science Laboratories, Sony International (Europe) GmbH, Hedelfinger Strasse 61, D-70327 Stuttgart, Germany, and Department of Inorganic Chemistry, Fritz-Haber-Institut der MPG, Faradayweg 4-6, D-14195 Berlin, Germany

Received: April 11, 2003; In Final Form: May 19, 2003

Gold nanoparticle/alkanedithiol films were prepared via layer-by-layer self-assembly. For the assembly process, dodecylamine-stabilized Au nanoparticles with an average size of 4 nm and alkanedithiols with different alkylene chain lengths (C_6, C_9, C_{12}, C_{16}) were used. The thickness of the films was determined by AFM and ranged between 26 and 34 nm. FE-SEM and TEM images indicate that the particle size within the film materials was similar to that of the dodecylamine-stabilized particles used for film preparation. The composition of the films was analyzed by XPS. The absence of the nitrogen signal indicated that the dodecylamine ligands were quantitatively exchanged by alkanedithiol molecules during film assembly. Two sulfur signals were observed, which could be assigned to sulfur bound to gold (S−Au) and to free thiol groups (S−H). As indicated by the relative signal intensities, about 60% of the alkanedithiol molecules were bound with both ends to the nanoparticles, whereas 40% were bound with only one thiol group. The C/S ratio was in good agreement with the stoichiometry of the alkanedithiol molecules. All films showed linear current−voltage characteristics. Conductivity measurements at variable temperature were consistent with an Arrhenius-type activation of charge transport. Using an activated tunneling model for describing the charge transport properties, we obtained an electron tunneling decay constant of $\beta_N = 0.61$ or 0.71, depending on the method used for data analysis. When the films were dosed with vapors of toluene and tetrachloroethylene, the resistance of the films increased reversibly. This response increased exponentially with increasing length of the alkanedithiol molecules. The chemical selectivity of the films corresponded essentially to the solubility properties of the alkanedithiol molecules.

1. Introduction

Recent efforts toward controlling the physical and chemical properties of nanostructured materials through molecular-level design have generated enormous interest in thin films comprised of organically encapsulated metal nanoparticles.[1] In several reports, it has been shown that the optical and electronic properties of such films can be tuned by varying the size of the metal particles[2−5] or the molecular weight and/or structure of the organic component.[6−12] For example, the charge transport in films from alkane-[13,14] and arenethiolate-[15] protected Au nanoparticles can be described as an activated tunneling process, which is strongly affected by variations of the size and the structure of the organic ligands. Brust and co-workers[7,8] reported on the layer-by-layer self-assembly of Au nanoparticle/alkanedithiol films and showed that the resistivity of such films strongly increased with increasing length of the dithiol linkers. Further, the optical and electrical properties of layer-by-layer self-assembled films comprised of Au or Ag nanoparticles and various organic compounds have been investigated by Natan and co-workers[9−11] and Murray and co-workers.[16,17]

An interesting application of metal nanopartice/organic films is their use as chemiresistor-type[12,16,18−24] or micrograviметric[16,21,25] gas sensors. As a first example, Wohltjen and Snow[18] reported that films from octanethiol-stabilized Au nanoparticles respond with a fast, reversible, and very sensitive increase of their resistance when exposed to vapors of toluene or tetrachloroethylene (TCE). Meanwhile, other reports appeared showing that the selectivity of such sensors can be tuned by introducing chemical functionality into the organic shell encapsulating the nanoparticles.[12−16,19−21,25] We reported recently on the fabrication and characterization of chemiresistors based on gold nanoparticle/dendrimer composite films.[22−24] The selectivity of such sensors was found to be controlled by the solubility properties and the size of the dendrimers used for film preparation.

The goal of our present study was to investigate systematically how the molecular structure, composition, conductivity, and vapor-sensing properties of alkanedithiol-interlinked gold nanoparticle films depend on the alkylene chain length. The films were prepared via layer-by-layer self-assembly, similar to the method described previously by Schiffrin and co-workers.[7] As the nanoparticle component, dodecylamine-stabilized gold nanoparticles[26] were used, which readily undergo ligand/linker exchange reactions. As alkanedithiol compounds, 1,6-hexanedithiol (C_6), 1,9-nonanedithiol (C_9), 1,12-dodecanedithiol (C_{12}), and 1,16-hexadecanedithiol (C_{16}) were used. To study the structure and chemical composition of the films, we employed atomic force microscopy (AFM), field-emission scanning electron microscopy (FE-SEM), transmission electron microscopy (TEM), and X-ray photoelectron spectroscopy (XPS). The charge tran-

† Part of the special issue "Arnim Henglein Festschrift".

* Corresponding author. E-mail: vossmeyer@sony.de. Fax: +49-711-5858-484. Phone: +49-711-5858-724.

§ Sony International (Europe) GmbH.

‡ Fritz Haber Institute of the MPG.

10.1021/jp030439o CCC: $25.00
Published on Web 06/28/2003

sport properties were characterized by measuring the conductivity of the films at variable temperature between 100 and 300 K. The results of these measurements are compared to previously reported data obtained from non-interlinked films of alkane*mono*thiol-stabilized Au nanoparticles[14] and single alkanedithiol molecules.[27] The vapor sensitivity of the films was investigated by dosing them with different solvent vapors while monitoring their resistance.

2. Experimental Section

2.1. Materials. *Chemicals.* Chemicals were purchased from Chempur, Fluka, Roth, Merck, Aldrich, and ABCR. All chemicals and solvents were reagent grade or of higher quality and used as received. Deionized water was purified using a Millipore Milli Q system (resistivity, 18.2 MΩ·cm). 1,6-Hexanedithiol (C_6) and 1,9-nonanedithiol (C_9) were purchased from Aldrich. 1,12-Dodecanedithiol (C_{12}), 1,16-hexadecanedithiol (C_{16}), and dodecylamine-stabilized gold nanoparticles were synthesized as described in the Supporting Information. The Au nanoparticles had a core size of 4.0 ± 0.8 nm, as determined by TEM.

Nanoparticle Films. The nanoparticle films were prepared using the layer-by-layer self-assembly method previously described by Bethell et al.[7] BK7 glass or oxidized silicon wafers were used as substrates. For investigating the electronic and vapor sensing properties, the glass substrates were equipped with interdigitated gold electrode structures (50 finger pairs, 10 μm width and 100 nm height, including a 5-nm titanium adhesion layer, 10 μm spacing, 1800 μm overlap). Prior to film deposition, the substrates were cleaned with acetone and 2-propanol and by application of an oxygen plasma (4 min at 30 W and 0.24 mbar). The substrates were then immersed into a solution of 50 μL of 3-aminopropyldimethylethoxysilane in 5 mL of toluene and heated to 60 °C for 30 min. After the substrates were washed with toluene, they were treated for 15 min with a solution of Au nanoparticles in toluene. The concentration of the particle solution corresponded to an absorbance of 0.4, measured at the maximum of the plasmon absorption band (λ_{max} = 514 nm; 2 mm path length). After the substrates were washed again with toluene, they were treated with linker solution, which contained 25 μmol of alkanedithiol in 5 mL of toluene. After 15 min, the substrates were washed with toluene, and then the treatment with particle and linker solutions (to which we refer as one "deposition cycle" in the following) was repeated 13 times. Accordingly, the film deposition was finished by treating the substrates with the solution of alkanedithiol, unless otherwise stated. The deposition of the gold particles was monitored by measuring the conductance of the films and their UV/vis spectra after each deposition cycle. Before such measurements, the films were briefly dried under a nitrogen stream.

Throughout this text, we use the following acronyms to denote the films according to the chain length of linker molecules they comprised: AuC_6, AuC_9, AuC_{12}, and AuC_{16}.

2.2. Apparatus. *UV/Vis Spectroscopy.* UV/vis spectra of the films were recorded with a Varian Cary 50 spectrophotometer. In the case of the spectra from the film materials, baseline correction was done using the BK7 substrates.

Microscopy (AFM, FE-SEM, TEM). A Digital Instruments Dimension 3100 atomic force microscope (AFM) with a Nanoscope IV controller was used to investigate the thickness and the morphology of the Au nanoparticle/alkanedithiol films. The film thickness was determined by imaging the edges of several scratches, which were produced by moving a needle across the film while applying gentle pressure. All images were acquired in "tapping mode". Further characterization of the film morphology was done using a Leo Gemini 1530 field-emission scanning electron microscope (FE-SEM). To characterize the particle sizes within the film material, we investigated two samples by transmission electron microscopy (TEM). For investigating the cross section of an Au nanoparticle/dodecanedithiol film, the silicon substrate supporting the film material was cut. Both pieces were then glued together (M-Bond 610, GATAN, Inc.), with the surfaces of the films facing each other. The resulting sandwiched sample was cut, polished, and ion-milled (GATAN PIPS 691 ion polishing system) until perforation at the silicon dioxide/film interface was observed. Cross-sectional images of the film material were taken using a Philips CM200 FEG TEM operated at 200 kV. For investigating a second sample, an Au nanoparticle/hexadecanedithiol film was scratched off the substrate. The resulting flakes were resuspended in toluene and dropped onto a carbon-coated TEM grid. The solvent was then removed with filter paper. The flakes were investigated using a Philips CM200 TEM.

X-ray Photoelectron Spectroscopy (XPS). These investigations were carried out using a modified LHS/SPECS EA200 MCD system equipped with a Mg Kα source (1253.6 eV, 168 W) and a He I/II source (21.22 and 40.82 eV). For XPS measurements, the pass energy of the analyzer was fixed to 48 eV. The binding energy scale of the system was calibrated using Au $4f_{7/2}$ = 84.0 eV and Cu $2p_{3/2}$ = 932.67 eV from foil samples. The film samples were mounted on an Au-plated stainless steel sample holder. The base pressure of the UHV analysis chamber was 1×10^{-10} mbar. Charging of the film samples was corrected using the visible Fermi edge of the ultraviolet photoelectron (UP) spectra (Supporting Information, Figure S-5), resulting in Au $4f_{7/2}$ positions at 84.1 eV. From all spectra, a Shirley background was subtracted before the peak fitting with a symmetric Gauss−Lorentz sum function was performed. For all peaks, a full width at half-maximum (fwhm) of 1.14 eV and a Gauss−Lorentz ratio of 0.64 (0 = pure Gauss, 1 = pure Lorentz) were applied. The spin−orbit splittings were set to 3.65 eV for Au 4f and 1.20 eV for the S 2p signals. The respective intensity ratios were kept at 4:3 (Au $4f_{7/2}$:Au $4f_{5/2}$) and 2:1 (S $2p_{3/2}$:S $2p_{1/2}$). The atomic ratios of the film materials were determined from the integral intensities of the signals, which were corrected by Scofield sensitivity factors modified for the instrument (C 1s = 1.00, S 2p = 1.67, Au 4f = 19.80). These factors were obtained from the literature[28] and verified by measurements of spin-coated alkanedithiol films and an Au_2S_3 sample.

Charge Transport Measurements. Current−voltage ($I-V$) measurements at variable temperatures were carried out using a home-built setup comprising a liquid nitrogen container, a computer-interfaced temperature controller (LakeShore 330), and a source/monitor unit (Hewlett-Packard, HP4142B). Before the measurements were started, the films were stored overnight in a vacuum (ca. 8 mbar) to enhance desorption of contaminants.

Vapor Dose−Response Measurements. The same instruments as described in ref 23 were used to perform in situ resistance measurements. The resistances of the films were monitored with an applied bias of about 0.1 V. Purified and dried air (dew point −70 °C) was used as carrier gas. As test vapors, we used toluene, tetrachloroethylene (TCE), 1-propanol, and water. All experiments were carried out at room temperature (ca. 22 °C).

3. Results and Discussion

3.1. Film Formation and Optical Characterization. As described in detail in the Experimental Section, all films were prepared via layer-by-layer self-assembly.[7] Figure 1 shows how the conductance of the films increased with the number of depo-

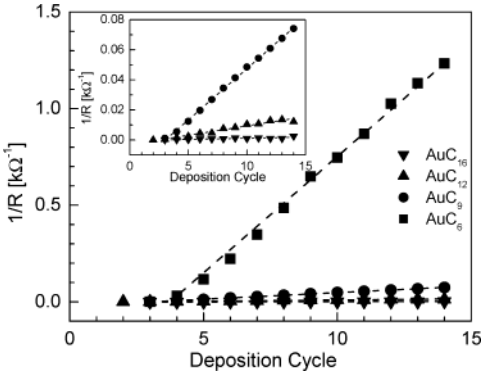

Figure 1. Conductance of the films AuC_6, AuC_9, AuC_{12}, and AuC_{16} measured after each deposition cycle. After the third or fourth cycle, the conductance increased linearly. The inset shows the data from the films AuC_{16}, AuC_{12}, and AuC_9 on a different scale.

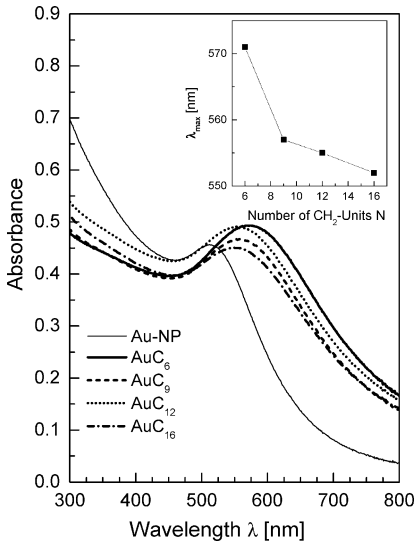

Figure 2. UV/vis spectra of the nanoparticle films and of the nanoparticle solution (Au−NP) used for film deposition. With decreasing length of the linker molecules, the plasmon band of the films became more pronounced and shifted further to the red, as shown in the inset.

sition cycles. A significant increase of conductance was measured only after the third or fourth deposition cycle, suggesting that, at this stage of film formation, a conductive network between the electrodes was formed. The linear increase of conductance reveals that, with each further deposition cycle, the same amount of nanoparticles was deposited. Accordingly, the UV/vis absorbance also increased linearly with the number of deposition cycles (Supporting Information, Figure S-2). The strong differences in the conductance of the films after 14 deposition cycles demonstrate that the interparticle distances were determined by the size of the linker molecules, as reported previously.[8]

The UV/vis spectra taken from the four nanoparticle films after 14 cycles are compared in Figure 2 with the spectrum from the particle solution (Au−NP) that was used for film preparation. Compared to the solution-phase spectrum, the plasmon absorption of the films ($\lambda_{max} \approx 560$ nm) is broadened and significantly shifted to longer wavelengths. This phenomenon is probably due to differences in the dielectric environment of the nanoparticles[29] as well as particle−particle interactions.[30] When comparing the spectra of the films, it is seen that, with decreasing length of the linker molecules, the plasmon band is shifted to longer wavelengths (see inset in Figure 2) and becomes more pronounced. Especially the spectrum of the C_6-

TABLE 1: Physicochemical Properties of Gold Nanoparticle/Alkanedithiol Films[a]

	E_a (kJ/mol)	d (±2) (nm)	R (kΩ)	σ_{RT} (1/Ω·cm)
AuC_6	5.05	26.2	0.574	3.73×10^{-2}
AuC_9	5.74	27.6	9.854	2.06×10^{-3}
AuC_{12}	5.99	33.8	72.131	2.30×10^{-4}
AuC_{16}	6.24	29.9	390.076	4.81×10^{-5}

[a] E_A, activation energy for charge transport; d, thickness of the films; R, resistance; σ_{RT}, room-temperature conductivity.

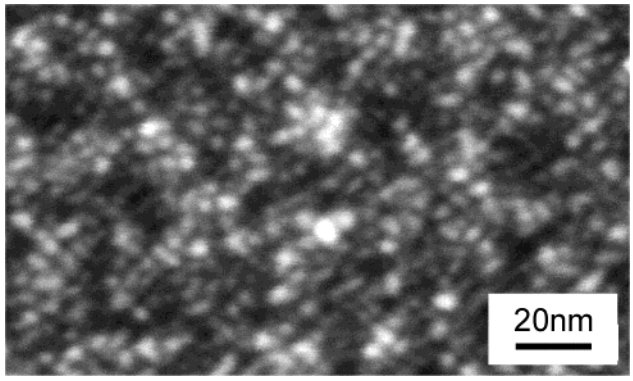

Figure 3. FE-SEM image of an AuC_{16} film deposited onto a silicon substrate. The granular film structure consists of particles with a diameter smaller than 10 nm.

interlinked film displays a significant red-shift. This result shows that particle−particle interactions became stronger with decreasing interparticle distances. This finding is in general agreement with results reported by Zamborini et al.,[16] who investigated the optical properties of Au nanoparticle films that were exposed to solvents. Similar observations have also been made by Mirkin and co-workers,[31] who investigated the aggregation of DNA-functionalized Au nanoparticles in aqueous solution.

3.2. Microscopy. The film thickness was determined by measuring the profiles of scratches with an AFM (Supporting Information, Figure S-3). As summarized in Table 1, the thickness of the films ranged between 26 and 34 nm. Information about the film morphology was obtained using electron microscopy. Figure 3 shows an FE-SEM micrograph taken from an AuC_{16} film deposited onto a silicon substrate. As can be seen, the film consists of nanoparticles having diameters <10 nm. Figure 4 (a and b) shows cross-sectional TEM images of an AuC_{12} film deposited onto a silicon substrate. The overview image shown in Figure 4a demonstrates that the nanoparticle film had a well-defined, uniform thickness. The high-resolution image shown in Figure 4b shows that the nanoparticles are distributed randomly across the film material. Since the image represents a projection of several nanoparticle layers, it is rather difficult to obtain reliable information on the particle sizes or shapes. However, the film thickness (ca. 30 nm) is comparable to that of the AuC_{12} film deposited on glass, which was measured by AFM (Table 1). Another possibility for investigating the film structure by TEM is to image flakes of the film materials which were scratched off the substrates. Figure 4c shows the TEM image of a flake from an AuC_{16} film. Similar to the case of Au nanoparticle/alkanedithiol networks precipitated from solution,[32] the particles formed a three-dimensional structure. At the rim of the flake, some individual particles with diameters between 3 and 6 nm are clearly recognized, which is in good agreement with the diameter of the particles used for film preparation, i.e., 4.0 ± 0.8 nm.

3.3. X-ray Photoelectron Spectroscopy (XPS). Overview XPS spectra of the four nanoparticle films showed signals from

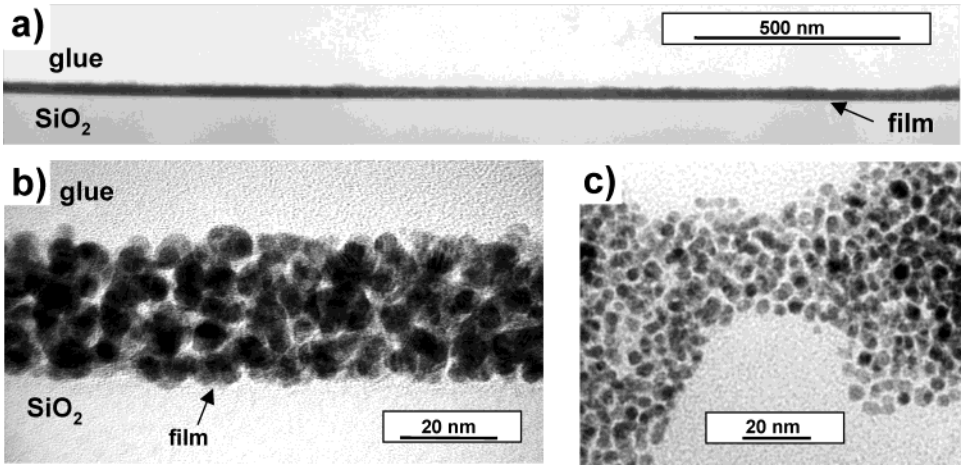

Figure 4. (a) Cross-sectional TEM image of an AuC_{12} film deposited onto a silicon substrate. (b) High-resolution image of the film's cross section, showing a random distribution of nanoparticles. The film thickness is about 30 nm. (c) TEM image of a flake from an AuC_{16} film. The particles seen at the rim of the flake have a diameter of 3−6 nm.

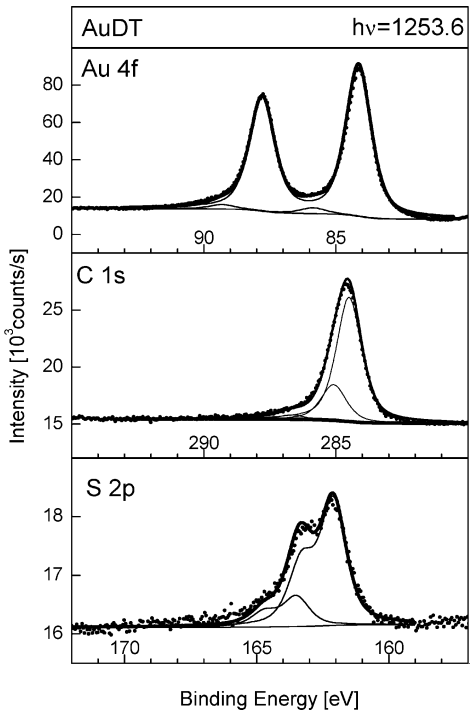

Figure 5. XPS spectra (Au 4f, C 1s, and S 2p region) of AuC_{12} deposited onto a silicon substrate. The two major components of the C 1s signal were assigned to carbon bound to sulfur (C−S, 285.2 eV) and to aliphatic carbon (C−C, 284.7 eV). The two spin−orbit split signals seen in the S 2p region were assigned to sulfur bound to the nanoparticles (S−Au, 162.1 eV) and to free thiol groups (S−H, 163.7 eV).

gold, carbon, and sulfur; no other elements were detected. Figure 5 shows the corresponding regions of the spectrum measured with an AuC_{12} film. The other films gave very similar spectra with respect to the peak shapes and their positions (a comparison of the spectra is given in the Supporting Information, Figure S-4). Due to the different stoichiometries of the linker compounds, significant differences were observed only regarding the relative signal intensities. In a few cases, XPS investigations of films from ligand-stabilized Au nanoparticles have been reported previously.[33,34] For example, XPS spectra from alkanethiol-stabilized gold nanoparticle films are comparable to those from the corresponding self-assembled alkanethiol monolayers (SAMs) on bulk gold surfaces.[33] The peak positions and shapes are similar, but the signal-to-noise ratio is higher in the case of the 3D nanoparticle structures.

The Au 4f signal shown in Figure 5 was fitted with two sum functions. The binding energy of the major component (Au $4f_{7/2}$ = 84.1 eV) is in agreement with results reported for alkanethiols assembled on gold nanoparticles and/or bulk gold substrates[35,36] as well as for bulk gold.[37] The very small contribution (<5% of the overall Au signal) around 85.8 eV (Au $4f_{7/2}$) might be due to atoms located at certain positions on the crystalline, faceted surfaces of the nanoparticles, e.g., at edges or corners. It is also possible that this signal is due to electrically disconnected Au particles, which charge up during the measurement.

The C 1s peak was fitted with three Gauss−Lorentz functions. The major contribution at a binding energy of 284.7 eV is characteristic for aliphatic carbon and is in agreement with data reported in the case of a C_{16} alkanethiol SAM on bulk Au(111).[38] According to the literature,[38,39] we assign the signal at ∼285.2 eV to carbon bound to sulfur. The third, minor component (<5% of the overall C 1s signal) at ∼286.9 eV is of unknown origin. It is noted that this peak is shifted by approximately the same energy as the minor Au signal.

The sulfur S 2p signal was fitted with two sum functions. According to previously published data, we assign the peak at ∼162.1 eV (S $2p_{3/2}$) to sulfur bound to Au nanoparticles (S−Au).[33−35,38] Further, the remaining signal at ∼163.7 eV (S $2p_{3/2}$) is assigned to sulfur of free thiol groups (S−H), which are not bound to the gold particles.[33,35] Signals from oxidized sulfur species, which would be expected at higher binding energies,[40] were not observed, even though the films were stored under ambient conditions for up to 5 weeks before the XPS experiments were conducted. This result demonstrates that even those sulfur atoms which are present as free thiol groups are quite resistant to oxidation. As a further result, we did not observe any signal in the N 1s region (around 400 eV). This suggests that, during the film preparation, the dodecylamine ligands which stabilized the Au nanoparticles in the solution phase were quantitatively exchanged by alkanedithiol linker molecules.

The atomic ratios of the three elements detected in the film materials were calculated from the integrals of the XPS signals. Table 2 summarizes the atomic ratios and the corresponding binding energies. The atomic ratios of Au, C, and S show linear dependencies on the number of methylene units in the linker chain, as depicted in Figure 6.

Ratios between different elements or species are given in Table 3. The ratios of carbon to sulfur (C 1s/S 2p) are in

TABLE 2: Atomic Ratios (in %) of Elements in the Film Material[a]

	Au 4f		S 2p		C 1s		
	Au + Au−S	Au*	S−Au	S−H	C−C	C−S	C*
BE (eV)	84.1	85.8	162.1	163.7	284.7	285.2	286.9
AuC_6	40.43	1.55	10.83	2.71	32.73	9.94	1.81
AuC_9	36.07	1.57	9.35	2.10	41.54	7.90	1.47
AuC_{12}	30.23	1.15	8.09	1.96	44.24	12.71	1.62
AuC_{16}	25.91	1.06	6.43	2.02	49.48	13.37	1.73
AuC_{12}, NP-terminated	36.77	1.08	6.49	1.88	40.43	11.14	2.21

[a] BE, binding energies of the different species. The origin of signal components marked with an asterisk (Au*, C*) is unknown. Atomic ratios of a "nanoparticle-terminated" AuC_{12} (NP-terminated) film are given for comparison.

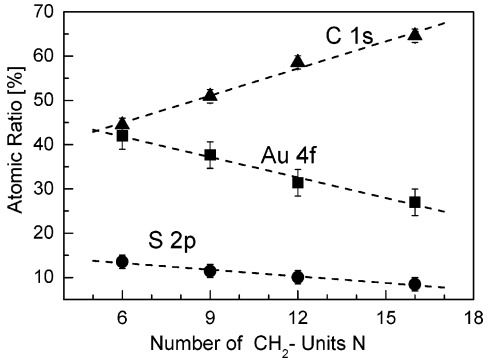

Figure 6. Atomic ratios of carbon, gold, and sulfur plotted vs the number *N* of methylene units present in the alkanedithiol linker molecules.

TABLE 3: Ratios between Elements or Species in the Films as Determined by XPS[a]

material	(C 1s + S 2p)/ Au 4f	C 1s/ S 2p	S−H/ S 2p	Au 4f/ S−Au
AuC_6	1.38	3.28	0.20	3.88
AuC_9	1.66	4.45	0.18	4.03
AuC_{12}	2.19	5.83	0.20	3.88
AuC_{16}	2.71	7.65	0.24	4.19
AuC_{12}, NP-terminated	1.64	6.42	0.22	5.83

[a] The C 1s/S 2p ratio corresponds to the stoichiometry of the linker molecules.

reasonable accordance with the stoichiometry of the linker molecules, confirming the reliability of the sensitivity factors used for carbon and sulfur [C/S stoichiometry (XPS experiment): C_6, 3.00 (3.28); C_9, 4.50 (4.45); C_{12}, 6.00 (5.83); C_{16}, 8.00 (7.65)]. The Au 4f/S 2p ratios are independent of the alkylene chain length (around 3.2 for all four films; not shown in Table 3), indicating that the particle/linker ratio is roughly the same in all four materials. The S−H/S 2p ratios listed in Table 3 represent the relative amounts of thiol groups which are not bound to the nanoparticles. As can be seen, in each film about 20% of the sulfur atoms are present as free thiol groups. This means that only about 60% of the linker molecules are attached on both ends to the nanoparticles.

The data presented in Table 3 were used to estimate the surface density of linker molecules on the nanoparticle cores. From the density of gold (which corresponds to 59 atoms/nm^3 in fcc gold), we calculate that one particle of 4 nm core size contains about 2000 atoms, of which about 725 are located at the surface. With an Au 4f/S−Au ratio of 4, this means that, for each surface-bound thiolate group, we count ~1.5 surface Au atoms on average. This value is half the value reported in the case of alkanethiol monolayers assembled on bulk Au(111) surfaces.[41] However, in case of alkanethiol-stabilized Au nanoparticles, Murray and co-workers[13] also reported an $Au_{surface}$/S ratio of 1.5. To explain this result, it was suggested that, in assemblies of alkanethiols on curved surfaces, steric crowding of the alkyl residues is much less than that on planar surfaces, and thus, the surface density of alkanethiol molecules on nanoparticle surfaces can be higher.

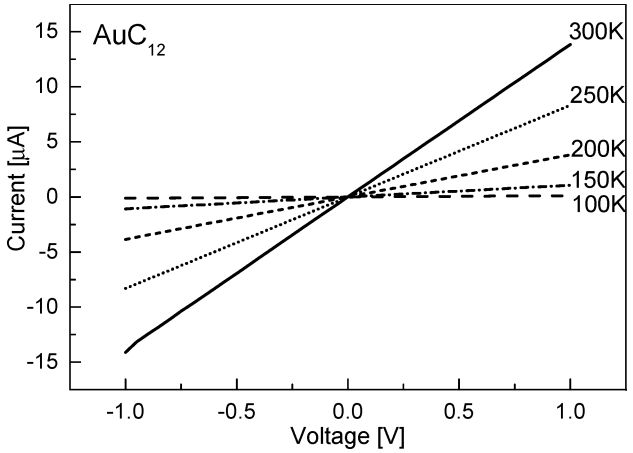

Figure 7. Current−voltage curves of the AuC_{12} film measured at the temperatures indicated.

To interpret the calculated surface density of linker molecules and the atomic ratios listed in Table 2 correctly, it has to be taken into account that the intensity of XPS signals decreases exponentially with the escape depth of the photoelectrons, which itself is in the range of the size of the nanoparticle cores.[42] Additionally, the film preparation was finished by depositing the organic component on top of the films. Therefore, the organic/gold ratios derived from the XPS signals are most likely overestimations. Also, the results presented above cannot clarify if the abundance of free thiol groups is mainly concentrated in the uppermost layer of linker molecules or if it is a bulk property of the films.

To get an impression of how strongly the XPS results were determined by assembling the linker molecules on top of the films, a "nanoparticle-terminated" AuC_{12} film was prepared by omitting the last step of linker assembly. The atomic ratios of this film and the relative ratios of the elements or species are also listed in Tables 2 and 3, respectively. A comparison with the data from the AuC_{12} linker-terminated film reveals a decrease of the (C 1s + S 2p)/Au 4f ratio by about 25%. The S−H/S 2p ratio of both films is very similar, indicating that only a small fraction of surface-bound thiol groups reacted when the last particle layer was assembled. It should be noted that also in the case of the particle-terminated film, no nitrogen was detected. This result indicates that the dodecylamine ligands were removed by washing the films after the nanoparticles were assembled.

3.4. Electronic Transport Properties. One major motivation of our present study was to provide information about the charge transport through alkanedithiol molecules assembled in three dimensions in Au nanoparticle films and to compare the results with data reported in the case of alkanedithiol molecules assembled on bulk substrates. Current−voltage (*I*−*V*) measurements of the four Au nanoparticle/alkanedithiol films revealed ohmic behavior within a voltage range of ±1.0 V and at temperatures between 100 and 300 K. Figure 7 shows the *I*−*V* curves of the AuC_{12} film measured at different temperatures. When the voltage range was extended to ±10 V, the AuC_6 film

gave nonlinear $I-V$ characteristics and showed an irreversible increase of conductivity. Under such conditions, the other films showed slight deviations from ohmic behavior, which became more apparent at low temperatures (e.g., 100 K). To work in the linear $I-V$ regime and to avoid damaging the films, all transport measurements reported below were performed within the ± 1.0 V range.

The room-temperature resistances of the films are listed in Table 1. These values are significantly lower than the resistances measured directly after the film preparation (compare Figure 1). This effect is explained by taking into account that freshly prepared films contained relatively large amounts of solvent (see below). Taking into account the thickness of the films and the geometry of the electrode structures, it is possible to translate the resistances into the room-temperature conductivities,[43] σ_{RT}. The values of σ_{RT} are also listed in Table 1.

For describing the conductivity of films from alkanethiol-stabilized gold nanoparticles, Murray and co-workers[13,14] used an activated tunneling model according to the following equation:

$$\sigma = \sigma_0 \exp[-\beta_N N] \exp[-E_A/RT] \quad (1)$$

In this expression, N is the number of carbon atoms in the alkane chain, E_A is the activation energy, R is the gas constant, and T is the absolute temperature. The first exponential expression describes the charge transport via tunneling of electrons from one particle core to another through the insulating barrier of organic material. The second exponential expression takes into account the thermal activation of charge carriers. To determine the activation energies E_A, the conductivities of the films were measured in the temperature range between 100 and 300 K. In Figure 8a, the logarithm of the conductivity is plotted vs $1/T$. From the slope of these curves, E_A can be determined according to eq 1. The obtained values, which are given in Table 1, increase with the chain length of the linker molecules. Schiffrin and co-workers[32] reported E_A values for AuC_5, AuC_6, and AuC_{12} films which deviate from the values reported here. However, these deviations can be explained by the different particle core sizes used in that previous study.

According to the granular metal theory,[44] $\ln(\sigma)$ was also plotted vs $T^{-0.5}$ (Supporting Information, Figure S-6). Within the temperature range considered here, the experimental data showed slightly stronger deviations from this model than from the Arrhenius model.

The electron tunneling decay constant β_N of eq 1 can be obtained by analyzing the room-temperature conductivities as a function of the linker chain length. In Figure 8b, the $\ln(\sigma_{RT})$ values are plotted vs N. If we tentatively fit the data linearly, the electronic decay constant β_N can be calculated from the slope of the fit according to eq 1.[45] This analysis gives $\beta_N = 0.71 \pm 0.1$. An alternative way of determining β_N is to extrapolate the plots shown in Figure 8a.[13,14] This procedure gives the intercepts $\{\ln(\sigma_0) - \beta_N N\}$, which are also plotted in Figure 8b. In this case, the slope of the linear curve fit gives $\beta_N = 0.61 \pm 0.1$.

Both values obtained for the electron tunneling decay constant are significantly lower than the values reported in the case of non-interlinked films of alkanethiol-stabilized Au nanoparticles.[14] This finding indicates that interlinking the nanoparticles with bifunctional alkanedithiol molecules enhances the conductivity of the films. The lower value we obtained (0.61) is in close agreement with the value of 0.57, which was reported by Lindsay and co-workers in the case of alkanedithiols assembled on bulk Au(111) substrates.[27] However, the value we calculated from the $\ln(\sigma_{RT})$ plot (0.71) falls between the values reported

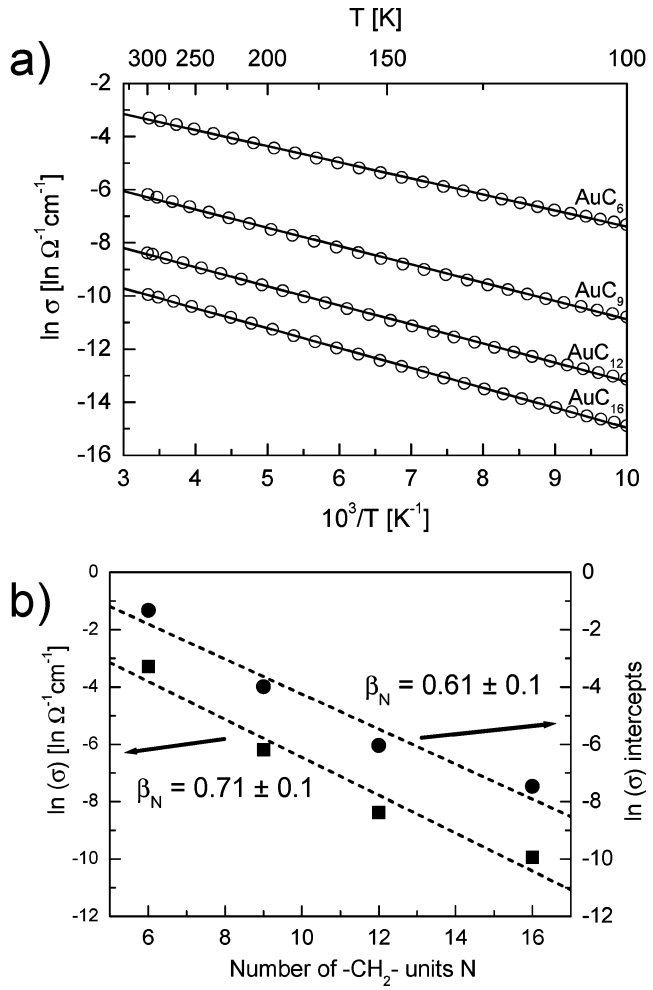

Figure 8. (a) Conductivity of the four film materials plotted as $\ln(\sigma)$ vs T^{-1}. Linear fits according to an Arrhenius-type activation of charge transport are shown as solid lines. According to eq 1, the slope of the fits was used to determine the activation energies E_A. (b) Plot of $\ln(\sigma_{RT})$ and the $\ln(\sigma)$ intercepts from part a vs the length of the linker molecules (expressed as the number N of methylene units). The electron tunneling decay constant β_N (0.71 and 0.61) was determined from the slope of the linear curve fits, as described in the text.

for electron tunneling through alkanedithiol molecules (0.57)[27] and alkanethiol molecules (1.2, 0.9, and 0.8).[14,46] This may indicate that charge transport in our films proceeds partly through the linker molecules (through-bond tunneling) and partly via interchain tunneling. This interpretation is supported by the XPS results, which indicate that only up to 60% of the alkanedithiol molecules act as linker molecules, whereas 40% are bound only with one end to the nanoparticles.

3.5. Vapor-Sensing Properties. Figure 9a shows how the resistance of the films increased when the four nanoparticle films were dosed with toluene vapor with a concentration of 800 ppm. In all cases, the response was fast and fully reversible. Within 3 s, 90% of the final response was reached ($t_{90} < 3$ s). In Figure 9b, the responses of the films (measured as the relative change of their resistance) to toluene vapor with various concentrations are plotted on a logarithmic scale vs N. As can be seen, the responses at a given concentration increased approximately exponentially with increasing number of methylene units. For discussing this result, it is interesting to compare the increase of sensitivity with the chemical composition of the films. As was seen in Figure 6, the atomic ratio of carbon increased linearly with the chain length of the linker molecules. Thus, if we assume that the number of sorption sites for toluene mole-

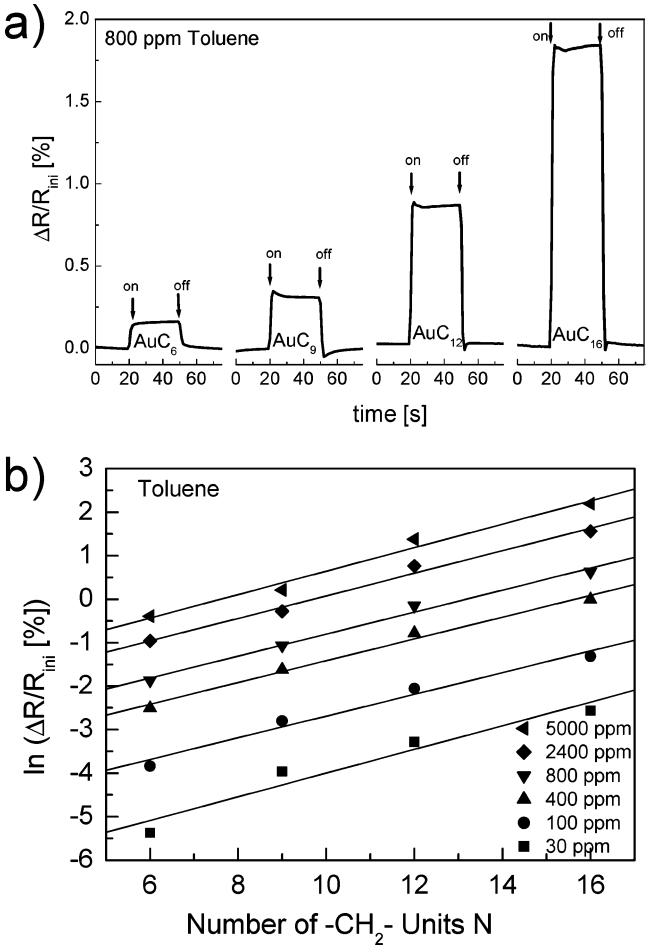

Figure 9. Response of the four nanoparticle films to toluene vapor. (a) Response signals measured as the relative change of resistance ($\Delta R/R_{ini}$). All films showed a fast and fully reversible response. The vapor concentration was 800 ppm. (b) Responses to toluene vapor with different concentrations, plotted as $\ln(\Delta R/R_{ini})$ vs the length of the linker molecules (expressed as the number of methylene units N). All measurements were performed at room temperature.

cules is determined by the amount of organic material, then our data suggest that the sensitivity of the films scales exponentially rather than linearly with the number of sorption sites. Results similar to those shown in Figure 9a,b were also obtained when the films were dosed with TCE vapor (data not shown).

To investigate the chemical selectivity, the films were dosed with vapors of toluene, TCE, 1-propanol, and water. These solvents have been used previously to study the sensitivity of films from octanethiol-stabilized Au nanoparticles.[18] They have similar vapor pressures (which makes them well suited for studying the chemical selectivity of sensor materials) and represent four different classes of analytes: 1, hydrophobic hydrocarbons; 2, chlorinated, hydrophobic hydrocarbons; 3, amphiphilic, H-bonding organic compounds; and 4, polar, H-bonding inorganic compounds. Figure 10 shows the response of the films. In each experiment, the concentration of the vapors was adjusted to 5000 ppm. The sensitivities to the hydrophobic vapors of toluene and TCE are quite similar. According to Figure 9b, an approximately exponential increase of the sensitivity with increasing length of the linker molecules is recognized. In the case of 1-propanol, the sensitivity of the films is very different. The sensitivity for this solvent first decreases with increasing linker length (AuC_6 to AuC_{12}) and then increases again (AuC_{16}). In the case of AuC_6, the sensitivity to 1-propanol is comparable to that of toluene and TCE. However, the other films are by far

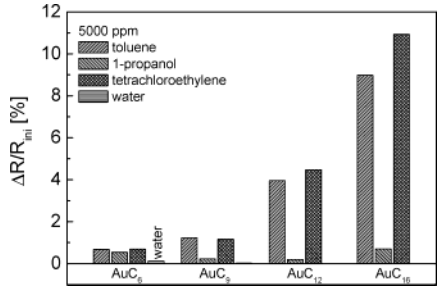

Figure 10. Responses of the four nanoparticle films to vapors of toluene, 1-propanol, tetrachloroethylene, and water. In each experiment, the vapor concentration was adjusted to 5000 ppm. Only in the case of AuC_6 was a weak response to water observed.

less sensitive to 1-propanol than toluene and TCE. Sensitivity to water vapor was observed only in the case of the AuC_6 film and was negligible in the case of the other films. In general, it can be summarized that the selectivity of the films was controlled mainly by the solubility properties of the linker molecules, similar to the behavior we reported previously in case of Au nanoparticle/dendrimer film resistors.[22]

The vapor-sensitivity of chemiresistors based on metal nanoparticle/organic composite films has been discussed previously in terms of swelling and changes of the dielectric environment of the nanoparticles.[16,19,20,23,24,47] The diffusion of vapor molecules into the pores of the films increases the average permittivity, because empty space is filled with vapor molecules. An increase of the permittivity should cause an increase of the conductivity because the activation energy and height of the potential well barriers are expected to decrease. However, the films investigated here responded with an increase of their resistance. This result suggests that film swelling, which leads to an increase of the interparticle distances, could be the dominant component of the sensing mechanism. To clarify the sensing mechanism more quantitatively and for understanding the exponential dependence of the response (to the hydrophobic analytes) on the linker chain length, further experiments are necessary. Such investigations should correlate the electrical responses with the actual amount of sorbed analyte.[21] In addition, the porosity of the films needs to be investigated, and theoretical considerations are required to model the swelling ability of the films as a function of the alkylene chain length.

4. Summary

Gold nanoparticle films interlinked with alkanedithiols of different alkylene chain length (C_6, C_9, C_{12}, and C_{16}) were prepared and characterized by AFM, FE-SEM, TEM, and XPS. The charge transport and vapor-sensing properties of these films were also investigated. The key results can be summarized as follows:

(a) Dodecylamine-stabilized Au nanoparticles and alkanedithiol linker molecules are well suited for the layer-by-layer assembly of interlinked Au nanoparticle films. FE-SEM and TEM images indicate that the size of the particles within the film material (ca. 3−6 nm) was similar to that of the dodecylamine-stabilized nanoparticles used for film preparation (4 ± 0.8 nm). This finding suggests that the particle size did not change during film deposition.

(b) XPS analysis of the films revealed that, during the film assembly process, the dodecylamine ligands were quantitatively exchanged by alkanedithiols. The C/S ratio was in good agreement with the stoichiometry of the linker molecules. The linker/Au ratio seems to be independent of the linker chain length. Only about 60% of the alkanedithiol molecules were

bound with both ends to the surface of the nanoparticles, the remainder being bound through only one thiol group.

(c) All films showed ohmic $I-V$ characteristics and Arrhenius-type activation of charge transport. Depending on the method used for data analysis, the electron-tunneling decay constant β_N was determined as 0.61 ± 0.1 and 0.71 ± 0.1. These values are significantly lower than the value reported for films from alkanethiol-stabilized nanoparticles ($\beta_N = 1.2$ or 0.9)[14] and thus confirm that interlinking the nanoparticles enhances the conductivity of the films. The decay constants reported here are similar to that measured in the case of single alkanedithiol molecules embedded in an alkanethiol host layer ($\beta_N = 0.57$).[27]

(d) When the films were dosed with vapors of toluene and TCE, a fast and fully reversible increase of their resistance was measured. At a given concentration, the response ($\Delta R/R_{ini}$) increased exponentially with increasing alkylene chain length. The chemical selectivity to different solvent vapors corresponded essentially to the solubility properties of the linker molecules. Our results suggest that swelling could be the dominant component of the sensing mechanism.

The fast response and the high sensitivity to volatile organic compounds (VOCs) make metal nanoparticle/organic films promising materials for sensor applications. To further investigate the sensing mechanism, it is necessary to correlate their electrical response with the actual uptake of analyte molecules. To do this, we are currently combining in situ microgravimetry and resistance measurements. In addition, we are employing in situ neutron reflectometry to acquire information about the analyte distribution across the sensor film and analyte-induced film swelling[47] as well as in situ spectroscopic techniques to study the analyte/linker interaction.

Acknowledgment. We thank Dr. Nadejda Krasteva and Dr. Nobuyuki Matsuzawa for helpful discussions, and Andrea Starke for supporting the synthesis of the linker molecules. Dr. Oliver Harnack is acknowledged for his support concerning the conductivity measurements. We thank Dr. William E. Ford for his kind assistance in preparing the manuscript. This project was supported by the BMBF, FKZ 03C0302A.

Supporting Information Available: Details of Au nanoparticle and linker synthesis; TEM and AFM images and XPS, UP, and UV−vis spectra; and discussion of electronic transport according to the granular metal theory. This material is available free of charge via the Internet at http://pubs.acs.org.

References and Notes

(1) Shipway, A. N.; Katz, E.; Willner, I. *Chem. Phys. Chem.* **2000**, *1*, 18−52.

(2) Snow, A. W.; Wohltjen, H. *Chem. Mater.* **1998**, *10*, 947−949.

(3) Beverly, K. C.; Sampaio, J. F.; Heath, J. R. *J. Phys. Chem. B* **2002**, *106*, 2131−2135.

(4) Leibowitz, F. L.; Zheng, W.; Maye, M. M.; Zhong, C.-J. *Anal. Chem.* **1999**, *71*, 5076−5083.

(5) Doty, R. C.; Yu, H.; Shih, C. K.; Korgel, B. A. *J. Phys. Chem. B* **2001**, *105*, 8291−8296.

(6) Fishelson, N.; Shkrob, I.; Lev, O.; Gun, J.; Modestov, A. D. *Langmuir* **2001**, *17*, 403−412.

(7) Bethell, D.; Brust, M.; Schiffrin, D. J.; Kiely, C. J. *J. Electroanal. Chem.* **1996**, *409*, 137−143.

(8) Brust, M.; Bethell, D.; Kiely, C. J.; Schiffrin, D. J. *Langmuir* **1998**, *14*, 5425−5429.

(9) Musick, M. D.; Keating, C. D.; Keefe, M. H.; Natan, M. J. *Chem. Mater.* **1997**, *9*, 1499−1501.

(10) Andres, R. P.; Bielefeld, J. D.; Janes, D. B.; Kolagunta, V. R.; Kubiak, C. P.; Mahoney, W. J.; Osifchin, R. G. *Science* **1996**, *273*, 1960.

(11) Musick, M. D.; Keating, C. D.; Lyon, L. A.; Botsko, S. L.; Pena, D. J.; Holliway, W. D.; McEvoy, T. M.; Richardson, J. N.; Natan, M. J. *Chem. Mater.* **2000**, *12*, 2869−2881.

(12) Foos, E. E.; Snow, A. W.; Twigg, M. E.; Ancona, M. G. *Chem. Mater.* **2002**, *14*, 2401−2408.

(13) Terrill, R. H.; Postlethwaite, T. A.; Chen, C.-H.; Poon, C. D.; Terzis, A.; Chen, A.; Hutchison, J. E.; Clark, M. R.; Wignall, G.; Londono, J. D.; Superfine, R.; Falvo, M.; Johnson, C. S., Jr.; Samulski, E. T.; Murray, R. W. *J. Am. Chem. Soc.* **1995**, *117*, 12537−12548.

(14) Wuelfing, W. P.; Green, S. J.; Pietron, J. J.; Cliffel, D. E.; Murray, R. W. *J. Am. Chem. Soc.* **2000**, *122*, 11465−11472.

(15) Wuelfing, W. P.; Murray, R. W. *J. Phys. Chem. B* **2002**, *106*, 3139−3145.

(16) Zamborini, F. P.; Leopold, M. C.; Hicks, J. F.; Kulesza, P. J.; Malik, M. A.; Murray, R. W. *J. Am. Chem. Soc.* **2002**, *124*, 8958−8964.

(17) Hicks, J. F.; Seok-Shon, Y.; Murray, R. W. *Langmuir* **2002**, *18*, 2288−2294.

(18) Wohltjen, H.; Snow, A. W. *Anal. Chem.* **1998**, *70*, 2856−2859.

(19) Zhang, H.-L.; Evans, S. D.; Henderson, J. R.; Miles, R. E.; Shen,T.-H. *Nanotechnology* **2002**, *13*, 439−444.

(20) Evans, S. D.; Johnson, S. R.; Cheng, Y. L.; Shen, T. *J. Mater. Chem.* **2000**, *10*, 183−188.

(21) Han, L.; Daniel, D. R.; Maye, M. M.; Zhong, C.-J. *Anal. Chem.* **2001**, *73*, 4441−4449.

(22) Krasteva, N.; Besnard, I.; Guse, B.; Bauer, R. E.; Muellen, K.; Yasuda, A.; Vossmeyer, T. *Nanoletters* **2002**, *2*, 551−5.

(23) Krasteva, N.; Guse, B.; Besnard, I.; Yasuda, A.; Vossmeyer, T. *Sens. Actuators B* **2003**, *92*, 137−143.

(24) Vossmeyer, T.; Guse, B.; Besnard, I.; Bauer, R. E.; Muellen, K.; Yasuda, A. *Adv. Mater.* **2002**, *14*, 238−2.

(25) Grate, J. W.; Nelson, D. A.; Skaggs, R. *Anal. Chem.* **2003**, *75*, 1868−1879.

(26) Leff, D. V.; Brandt, L.; Heath, J. R. *Langmuir* **1996**, *12*, 4723−4730.

(27) Cui, X. D.; Primak, A.; Zarate, X.; Tomfohr, J.; Sankey, O. F.; Moore, A. L.; Moore, T. A.; Gust, D.; Nagahara, L. A.; Lindsay, S. M. *J. Phys. Chem. B* **2002**, *106*, 8609−8614.

(28) Briggs, D.; Seah, M. P. *Practical Surface Analysis*, 2nd ed.; Wiley: Chichester, 1990; pp 635−638.

(29) Underwood, S.; Mulvaney, P. *Langmuir* **1994**, *10*, 3427−3430.

(30) Heath, J. R.; Knobler, C. M.; Leff, D. V. *J. Phys. Chem. B* **1997**, *101*, 189−197.

(31) Storhoff, J. J.; Lazarides, A. A.; Mucic, R. C.; Mirkin, C. A.; Letsinger, R. L.; Schatz, G. C. *J. Am. Chem. Soc.* **2000**, *122*, 4640−4650.

(32) Brust, M.;Bethell, D.; Schiffrin, D. J.; Kiely, C. J. *Adv. Mater.* **1995**, *7*, 795−797.

(33) Bourg, M.-C.; Badia, A.; Lennox, R. B. *J. Phys. Chem. B* **2000**, *104*, 6562−6567.

(34) Maye, M. M.; Luo, J.; Lin, Y.; Engelhard, M. H.; Hepel, M.; Zhong, C.-J. *Langmuir* **2003**, *19*, 125−131.

(35) Castner, D. G.; Hinds, K.; Grainger, D. W. *Langmuir* **1996**, *12*, 5083−5086.

(36) Chenakin, S. P.; Heinz, B.; Morgner, H. *Surf. Sci.* **1999**, *421*, 337−352.

(37) Heister, K.; Zharnikov, M.; Grunze, M.; Johansson, L. S. O. *J. Phys. Chem. B* **2001**, *105*, 4058−4061.

(38) Cavallieri, O.; Oliveri, L.; Dacca, A.; Parodi, R.; Rolandi, R. *Appl. Surf. Sci.* **2001**, *175−176*, 357−362.

(39) Beamson, G.; Briggs, D. High-resolution XPS of organic Polymers: the Scienta ESCA300 database, 1992.

(40) Freeman, T. L.; Evans, S. D.; Ulman, A. *Langmuir* **1995**, *11*, 4411−4417.

(41) Widrig, C. A.; Alves, C. A.; Porter, M. D. *J. Am. Chem. Soc.* **1991**, *113*, 2805−2810.

(42) Seah, M. P.; Dench, W. A. *Surf. Interface Anal.* **1979**, *1*, 2.

(43) The conductivities of the materials (σ_{RT}) were calculated using $\sigma_{RT} = g/[(2n - 1)ldR]$, with $n = 50$, number of electrode finger pairs; $g = 10$ μm, gap between electrodes; $l = 1800$ μm, overlap length of electrode fingers; and $d =$ thickness of the film as determined by AFM (see Table 1). For all films, the thickness of the films was below the height of the electrodes, i.e., 100 nm.

(44) Abeles, B.; Sheng, P.; Coutts, M. D.; Arie, Y. *Adv. Phys.* **1975**, *24*, 407−461.

(45) The dependence of E_A on the number of methylene units was empirically approximated using the values listed in Table 1. We obtained $E_{A(N)} = 4.54$ kJ mol^{-1} + 0.11 kJ mol^{-1} × N. With $\ln(\sigma_{RT}) = \ln(\sigma_0) - (4.54 \text{ kJ mol}^{-1}/RT) - N\{\beta_N - (0.11 \text{ kJ mol}^{-1}/RT)\}$, we determined β_N from the slope of the linear fit, shown in Figure 10b as $\beta_N = 0.71$.

(46) Cui, X. D.; Zarate, X.; Tomfohr, J.; Sankey, O. F.; Primak, A.; Moore, A. L.; Moore, T. A.; Gust, D.; Harris, G.; Lindsay, S. M. *Nanotechnology* **2002**, *13*, 5−14.

(47) Krasteva, N.; Krustev, R.; Yasuda, A.; Vossmeyer, T. *Langmuir* **2003**, in press.